Available online at www.sciencedirect.com
ScienceDirect
Journal of the European Ceramic Society 31 (2011) 2145–2153
www.elsevier.com/locate/jeurceramsoc

# Pressureless sintered in situ toughened $ZrB_2$–SiC platelets ceramics

D. Sciti *, L. Silvestroni, V. Medri, S. Guicciardi

*CNR-ISTEC, Institute of Science and Technology for Ceramics, Via Granarolo 64, I-48018 Faenza, Italy*

Received 28 December 2010; accepted 29 April 2011
Available online 31 May 2011

**Abstract**

$ZrB_2$–SiC composite ceramics were densified by pressureless sintering with addition of $Si_3N_4$ or $MoSi_2$ at temperatures that induced SiC anisotropic growth from particles to platelets, within a $ZrB_2$ matrix with rounded grains. $Si_3N_4$ addition resulted in the formation of large amounts of liquid phase which enhanced mass transfer mechanisms in terms of matrix grain growth and homogeneous distribution of SiC platelets having an aspect ratio of 3. On the contrary, $MoSi_2$ helped the densification with local formation of liquid phases leading to a finer matrix with finer SiC platelets, though more agglomerated and with a lower aspect ratio (about 2). These different microstructures had very different fracture properties values, namely a toughness of 3.8 MPa $m^{1/2}$ and a strength of 300 MPa for the $Si_3N_4$-doped composite; toughness of 5 MPa $m^{1/2}$ and strength of 410 MPa for the $MoSi_2$-doped one.


*Keywords:* Borides; Platelets; Sintering; Microstructure; Toughness and toughening

## 1. Introduction

Zirconium diboride-based materials are currently considered a class of promising materials for several applications, in particular in the aerospace sector. In the last five years, research has focused on the fabrication of dense composites possessing high strength (500–1000 MPa).[1–4] However, the low fracture toughness remains one of the major concerns for the application of these materials under severe environmental conditions. Commonly, the fracture toughness of various $ZrB_2$-based composites is hardly higher than 4.5 MPa $m^{1/2}$. This can be seen in Fig. 1 (white columns) which shows the fracture toughness of several $ZrB_2$-based materials produced in our labs. They embrace both monolithic $ZrB_2$, i.e. only containing sintering agents below 5 vol%, and composites containing particulates of SiC.[4–7] The fracture toughness of these materials was measured with the same chevron notched beam (CNB) technique. As it can be seen the values range from about 2.9 to 4.0 MPa $m^{1/2}$ for unreinforced materials and from 3.8 to 4.6 for SiC particle reinforced $ZrB_2$.[4–7] Other toughness values reported in the literature were not included in the comparison as they were very often obtained with a different testing technique, and it is widely recognized that the testing technique can have a large impact on the measured toughness value.[8]

From Fig. 1, it is particularly evident that often the addition of particles does not represent an effective strategy for a major toughness improvement. In case of SiC particles, for example, it has been shown that residual tensile stresses are developed in the $ZrB_2$ matrix, due to the difference of thermal expansion coefficient between SiC and $ZrB_2$.[9] As a result, particle-reinforced $ZrB_2$–SiC materials are often as brittle as other $ZrB_2$-based composites even if they display significant increase of hardness and strength.

Spherical reinforcement can be efficaciously substituted by elongated reinforcement. The potential advantages of elongated secondary phases over particulate-reinforced systems include more effective toughening mechanisms such as enhanced crack deflection and load-carrying capability. In addition, other toughening mechanisms, such as crack bridging and pullout, are possible. Indeed, significant increases of fracture toughness have been recently obtained through addition of SiC whiskers[10–12] or carbon fibers.[13] Also for the SiC whisker-reinforced $ZrB_2$ composites and SiC chopped fiber-reinforced composites produced in our labs a significant toughness improvement has been obtained[14,15] especially when the content of whisker or fiber was around 20 vol%, see Fig. 1 (dark grey columns). However, it must be mentioned that processing this kind of composites requires special care, as the reinforcement can be severely

* Corresponding author. Tel.: +39 0546 699748; fax: +39 0546 46381.
*E-mail address:* diletta.sciti@istec.cnr.it (D. Sciti).

0955-2219/$ – see front matter © 2011 Elsevier Ltd. All rights reserved.
doi:10.1016/j.jeurceramsoc.2011.04.040

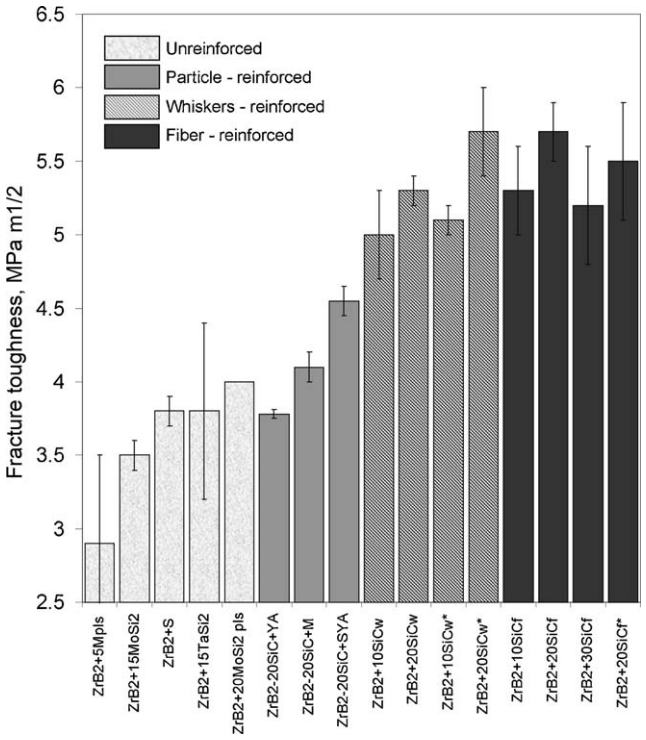


Fig. 1. Comparison of the fracture toughness values of several $ZrB_2$-based materials produced in our labs, un-reinforced (from Refs.[4–7]), particle-reinforced (from Refs.[4–7]), whiskers reinforced (from Refs.[14,15]) and chopped-fibers reinforced composites (from Refs.[14,15]). All the values were obtained by the chevron notched beam technique. Error bars represent ±1 standard deviation.

degraded if the sintering temperature is higher than 1750 °C: SiC whiskers tend to agglomerate and transform into particles, SiC chopped fibers undergo decomposition and progressive detachment from the matrix. This implies that only pressure-assisted techniques (hot pressing, spark plasma sintering) can be used to effectively sinter these composites, which means that the possibility to obtain reinforced materials by pressureless sintering is highly reduced or very difficult when these kinds of reinforcement are introduced. On this line, it is worth mentioning the notable increase of fracture toughness that has been recently obtained through development of elongated $ZrB_2$ grains by pressureless sintering at $T = 2200$ °C.[16]

In this work, the main objective was to explore the possibility to obtain tough $ZrB_2$–SiC composites in which SiC platelets, an intermediate reinforcement geometry between particles and fibers, are developed in situ by pressureless sintering. The main advantage of pressureless sintering over pressure-assisted sintering is the possibility to produce near-net shaped components. The direct incorporation of commercially available SiC platelets would in fact require the use of pressure-assisted techniques, as these large reinforcements would hinder the matrix densification.

$ZrB_2$ materials containing 20 vol% SiC platelets were produced by starting either from α- or β-SiC particles. The pressureless sintering cycle was set in order to obtain coalescence and anisotropic growth of SiC starting particles, which normally occurs at temperatures higher than 1900 °C. This anisotropic growth offers the possibility to obtain an in situ reinforcement and, potentially, an increase of fracture toughness.[17] Different sintering aids, such as $Si_3N_4$ and $MoSi_2$, are used and their effect on microstructure and fracture properties is compared.

## 2. Experimental procedure

The following compositions were selected for the present study:

$ZrB_2 + 5$ vol% $MoSi_2 + 2$ vol% α-SiC particles, labeled as ZMα.
$ZrB_2 + 5$ vol% $MoSi_2 + 20$ vol% β-SiC particles, labeled as ZMβ.
$ZrB_2 + 5$ vol% $Si_3N_4 + 20$ vol% β-SiC particles, labeled as ZSβ.

Commercial powders were used to prepare the ceramic composites:

$ZrB_2$ Grade B (H.C. Starck, Germany), specific surface area 1.0 $m^2/g$, impurities: 0.25 wt% C, 2 wt% O, 0.25 wt% N, 0.1 wt% Fe, 0.2 wt% Hf, particle size range 0.1–8 μm; α-SiC (Starck UF-25, Germany), specific surface area 23–26 $m^2/g$, impurities: 2.5 wt% O, mean particle size 0.45 μm; β-SiC (Starck BF-12, Germany), specific surface area 11–13 $m^2/g$, impurities: 0.88 wt% O mean particle size 0.60 μm; tetragonal $MoSi_2$ (Aldrich, Germany), specific surface area 1.60 $m^2/g$, impurities: 1 wt% O, mean particle size 1 μm; α-$Si_3N_4$ Baysind (Bayer, Germany), specific surface area 12.2 $m^2/g$, impurities: 1.5 wt% O, mean particle size 0.15 μm.

The powder mixtures were ball milled for 24 h in absolute ethanol using $ZrO_2$ media. Subsequently the slurries were dried in a rotary evaporator. The pellets were prepared by uniaxial pressing followed by cold isostatic pressing under 250 MPa. These specimens were subsequently pressureless sintered in a resistance-heated graphite furnace (Onyx Furnace 22001 C, LPA DVM, Seyssinet, France) under a flowing argon atmosphere (∼0.1 MPa) with heating rate of 600 °C/h at temperatures of 2100–2150 °C and holding times of 120 min. After the dwelling time, free cooling was set.

The bulk densities were measured by Archimedes' method. Crystalline phases were identified by X-ray diffraction (Siemens D500, Germany). The fractured and polished surface of the samples were analyzed by scanning electron microscopy (SEM, Cambridge S360, Cambridge, UK) and energy dispersive spectroscopy (EDS, INCA Energy 300, Oxford Instruments, UK). TEM samples were mechanically polished to a thickness of about 150 μm and punched out 3 mm in diameter by an ultrasonic cutter. After mirror polishing on both the surfaces, it was created a dimple to about 10 μm and then further ion beam thinned until small perforations were observed by optical microscopy.

The Vickers hardness (HV1.0) was measured on polished surfaces with an applied load of 9.81 N. The fracture toughness ($K_{Ic}$) was evaluated using chevron notched beam (CNB) in flexure. The test bars, 25 mm × 2 mm × 2.5 mm (length by width by

thickness, respectively), were notched with a 0.1 mm-thick diamond saw; the chevron-notch tip depth and average side length were about 0.12 and 0.80 of the bar thickness, respectively. The specimens were fractured using a semi-articulated silicon carbide four-point fixture with a lower span of 20 mm and an upper span of 10 mm using a screw-driven load frame (Instron mod. 6025). The specimens, three for each composite, were loaded with a crosshead speed of 0.05 mm/min. The "slice model" equation of Munz and Fett[18] was used to calculate $K_{Ic}$. On the same machine and with the same fixture, the flexural strength was measured at room temperature ($\sigma_{RT}$) and at 1200 °C in air ($\sigma_{1200}$); for each material and temperature, five bars were tested.

## 3. Results

### 3.1. Microstructure

ZMα and ZMβ: The sintering temperature used for these materials was set higher than the temperature required for the densification in order to induce the elongation of the SiC particles. Previous studies have indeed shown that temperatures around 1850 °C are sufficient to get 95% dense materials.[6] The final relative density of ZMα and ZMβ were around 98% of the theoretical density (Table 1). A subsequent SEM analysis confirmed that the level of porosity was lower than 3%. The crystalline phases detected by X-ray diffraction in ZMα and ZMβ were $ZrB_2$, a mixture of SiC 6H and 4H polytypes, MoB, traces of $MoSi_2$ and $Mo_{4.8}Si_3C_{0.6}$. It must be mentioned that in the composite containing α-SiC, ZMα, the SiC polytypes detected after sintering were the same of the starting powder. In case of ZMβ, as well as ZSβ, the presence of polytypes was instead a consequence of the irreversible β → α transformation occurring at temperatures above 1900 °C.[19] Fracture surfaces reported in Fig. 2a and b show that ZMα and ZMβ had a fine microstructure and failed mainly intergranularly, without any evidence of SiC reinforcement pullout. In the polished sections, both compositions exhibited a $ZrB_2$ matrix containing large SiC platelets, see Fig. 2c, with an aspect ratio (AR) around 2, Table 1. Starting from either α- or β-silicon carbide powder, the adopted thermal treatment efficaciously transformed the original SiC particles in SiC platelets. ZMα and ZMβ showed very similar microstructure, except by the fact that both $ZrB_2$ and SiC had a finer mean grain size in ZMα, due to the smaller SiC starting powder, which exerted higher compelling forces on the matrix. The matrix grains displayed a core–shell morphology, where the core was $ZrB_2$ and the shell contained also traces of molybdenum (Fig. 3a).[20] The secondary phases observed by SEM analysis were ZrC, MoB and very small amount of residual $MoSi_2$ (Fig. 3a and b). At the interface SiC–$ZrB_2$–MoB and at the apical regions of MoB, triple points containing Zr, Mo, Si, B or C and O were detected. The presumed compositions are $(Mo,Zr)_5SiB_2$ and $Mo_{4.8}Si_3C_{0.6}$, according to X-ray diffraction pattern and previous studies on similar composites.[20] In ZMβ, TEM analysis revealed clean grain boundaries between SiC platelets and $ZrB_2$, Fig. 4 a, whilst intergranular glassy phases containing Si, O, Mo, Zr, B were sometimes observed at $ZrB_2$/$ZrB_2$ grain boundaries, Fig. 4b and c.

Table 1
Label, composition, density, most relevant microstructural parameters and mechanical properties of the investigated materials. Mean ± 1 standard deviation, when appropriate. $K_{Ic}$: fracture toughness; $\sigma_{RT}$ and $\sigma_{1200}$: flexural strength at room temperature and 1200 °C, respectively.

| Label | Starting composition (vol%) | Th. density (g/cm$^3$) | Bulk density (g/cm$^3$) | Rel. density (%) | $ZrB_2$ m.g.s. (μm) | SiC m.g.s. (AR) (μm) | HV1.0 (GPa) | $K_{Ic}$ (MPa m$^{1/2}$) | $\sigma_{RT}$ (MPa) | $\sigma_{1200}$ (MPa) | Ref. |
|---|---|---|---|---|---|---|---|---|---|---|---|
| ZM | $ZrB_2$ + 5$MoSi_2$ | 6.11 | 5.86 | 96.0 | 2.6 | – | 15.2 ± 1.0 | 2.9 ± 0.1 | 570 ± 50 | 530 ± 90 | 5 |
| ZMα | $ZrB_2$ + 5$MoSi_2$ + 20SiC | 5.53 | 5.42 | 98.1 | 3.1 | 2.2 (1.9) | 14.9 ± 0.7 | 4.7 ± 0.1 | 350 ± 80 | – | This work |
| ZMβ | $ZrB_2$ + 5$MoSi_2$ + 20SiC | 5.53 | 5.44 | 98.4 | 3.8 | 2.6 (2.3) | 13.8 ± 0.2 | 5.0 ± 0.1 | 410 ± 40 | 380 ± 30 | This work |
| ZS | $ZrB_2$ + 5$Si_3N_4$ | 5.96 | 5.73 | 96.1 | 3.0 | – | 13.4 ± 0.6 | 3.8 ± 0.1 | 600 ± 90 | 250 ± 10 | 7 |
| ZSβ | $ZrB_2$ + 5$Si_3N_4$ + 20SiC | 5.40 | 5.24 | 96.4 | 8.9 | 6.2 (2.9) | 13.2 ± 0.2 | 3.8 ± 0.1 | 300 ± 40 | – | This work |

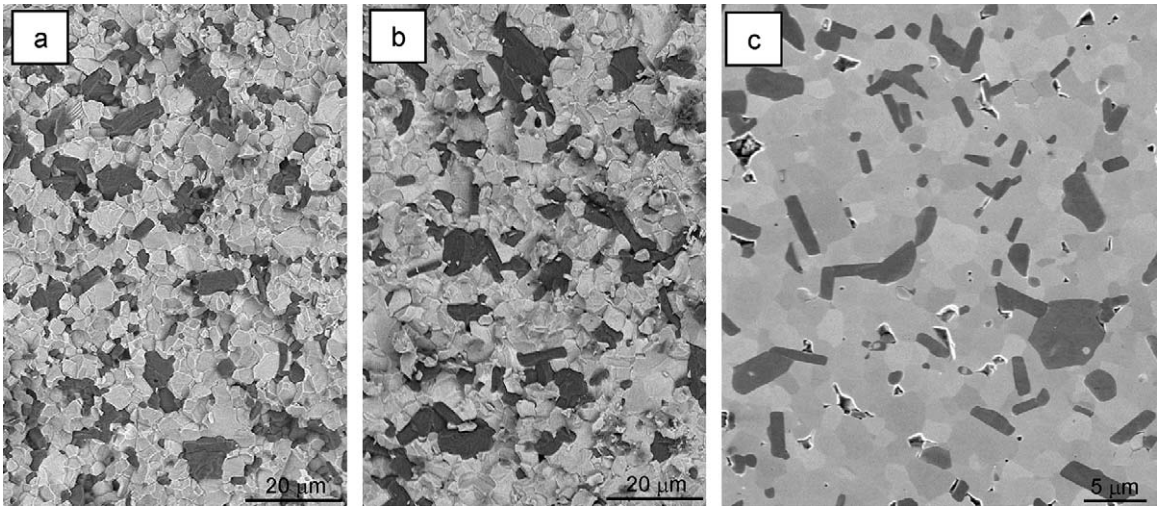


Fig. 2. Fractured surface of (a) ZMα, (b) ZMβ. In (c), polished surface of ZMβ.

ZSβ: As for the previous samples, the sintering temperature was set higher than that normally required to get a full densification (∼1700 °C) with no grain coarsening, in order to enhance the development of SiC platelets. After sintering, ZSβ reached a final relative density of 96%. According to X-ray diffraction, the crystalline phases were a mixture of α-SiC polytypes 6H and 4H. Crystalline phases deriving from silicon nitride, if present, were below the detection limit of the instrument.[21] Fractured and polished surfaces reported in Fig. 5a and b show that ZSβ had a quite coarse microstructure and failed mainly transgranularly, i.e. very differently from the previous samples. Also in this case, no pullout of the SiC reinforcement was observed. In the polished section, it can be seen that the SiC platelets developed in this composite had a larger aspect ratio (∼3) than that of the $MoSi_2$-doped composites, see Table 1. Detailed SEM analysis revealed that beside $ZrB_2$ and α-SiC platelets, traces of secondary phases such as BN, ZrN, $ZrSi_2$, graphite, $B_4C$ and residual $Si_3N_4$ were detected (Fig. 6a). Glassy pockets were also found adjacent to SiC platelets and from these pockets wetted interfaces could be occasionally observed especially along $ZrB_2$/$ZrB_2$ grain boundaries (Fig. 6b). EDS on these regions revealed an oxygen enrichment, as indicated in Fig. 6c. TEM analysis focused on $ZrB_2$/SiC platelet interfaces generally revealed clean interfaces (Fig. 7). This was unexpected as $ZrB_2$–SiC particles materials sintered at lower temperature with $Si_3N_4$ as sintering aid displayed a very different microstructure, with both $ZrB_2$ grains and SiC particles embedded in a residual Si–O–N–Zr glassy phase.[7,14,15]

### 3.2. Mechanical properties

ZMα and ZMβ: The mechanical properties are summarized in Table 1. For comparison, the properties of a baseline unreinforced material (ZM) with composition $ZrB_2$ + 5 vol% $MoSi_2$ sintered at 1900 °C are also reported.[6] Starting from a baseline hardness value of 15.2 GPa, it can be seen that the hardness value is unchanged for ZMα but tends to decrease in ZMβ. A notable increase of toughness, from 2.9 to 4.7–5 MPa $m^{1/2}$, was instead observed for both composites in comparison with the baseline material. Conversely, the room temperature flexu-

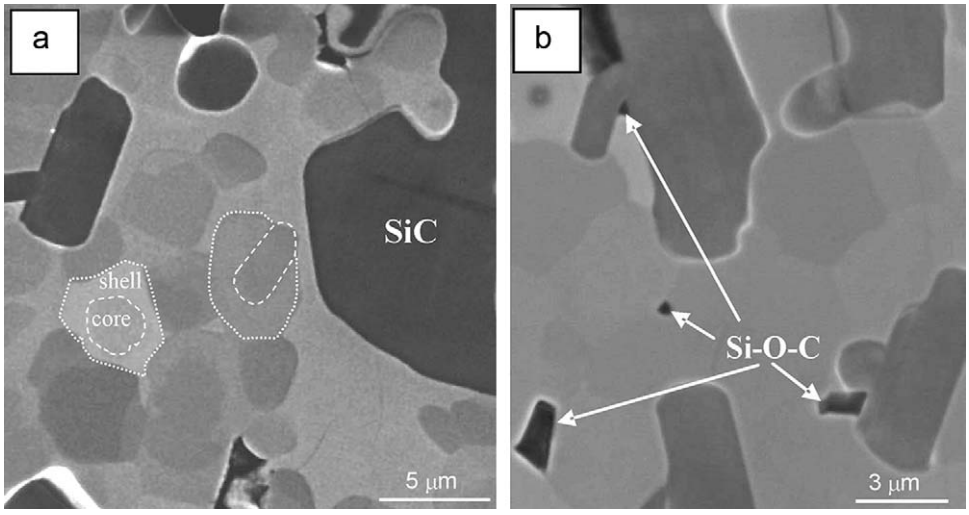


Fig. 3. SEM images of ZMβ showing (a), the core–shell morphology of $ZrB_2$ grains, (b) an enlarged view of the secondary low density phases based on Si–O–C.

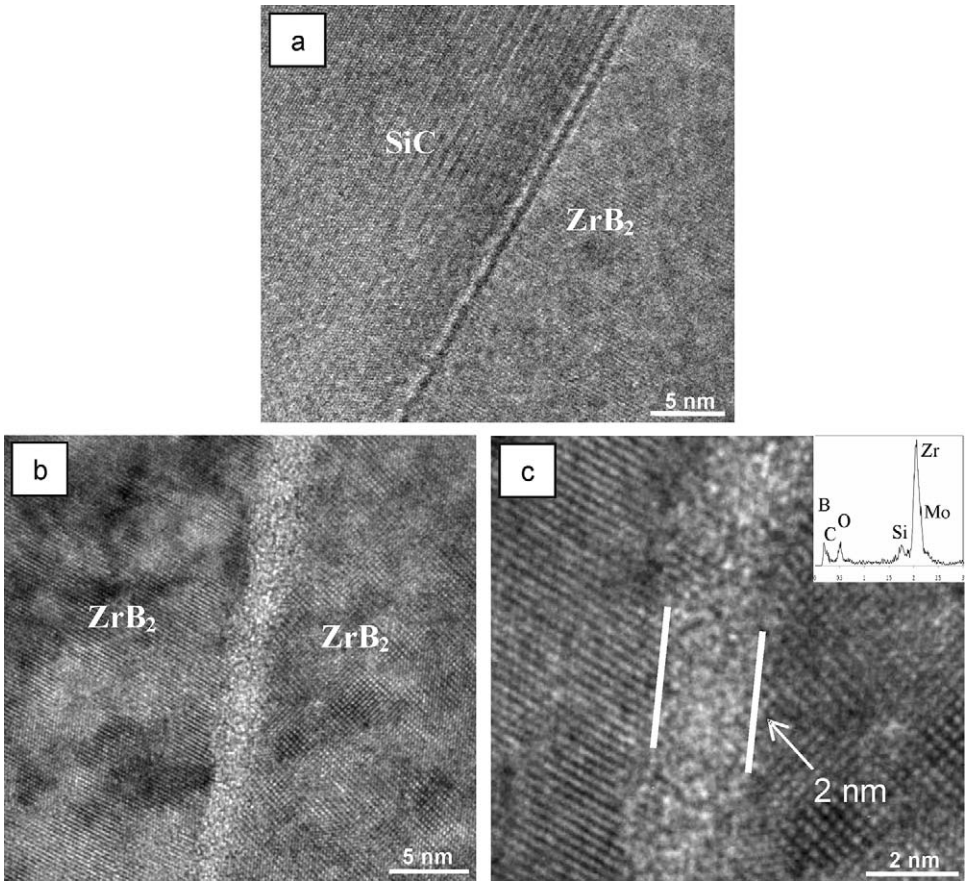


Fig. 4. TEM images showing in (a) a clean $ZrB_2$/SiC interface in ZMβ. In (b) an amorphous film between two $ZrB_2$ grains. In (c) the corresponding filtered FT and the EDS spectrum of the amorphous layer.

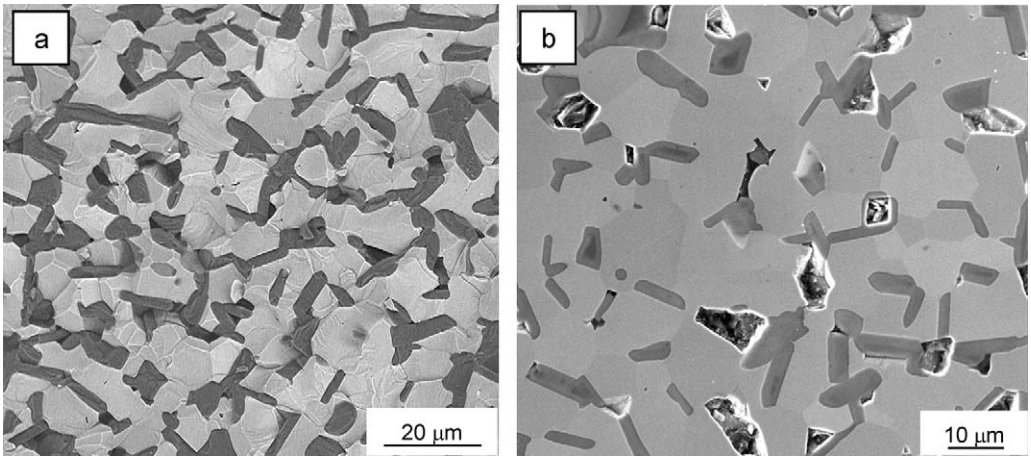


Fig. 5. (a) Fractured and (b) polished surface of ZSβ.

ral strength decreased from 570 MPa in the reference material to 410 MPa in ZMβ and 350 MPa in ZMα. When tested at 1200 °C, the flexural strength of ZMβ was just slightly lower than that at room temperature.

ZSβ: In Table 1, the mechanical properties of ZSβ are compared with a reference material (ZS) sintered at 1700 °C, i.e. 400 °C lower than the material of the present work.[7] Despite the very different microstructures, hardness and fracture toughness were practically the same both in the platelet-containing composite and in the unreinforced matrix. The fracture toughness of ZSβ, notwithstanding the presence of SiC platelets, was not substantially different from the typical values of monolithic or particle-reinforced $ZrB_2$-based materials developed so far, see Fig. 1 (white columns). The room temperature strength decreased from 600 MPa (ZS) to 300 MPa (ZSβ).

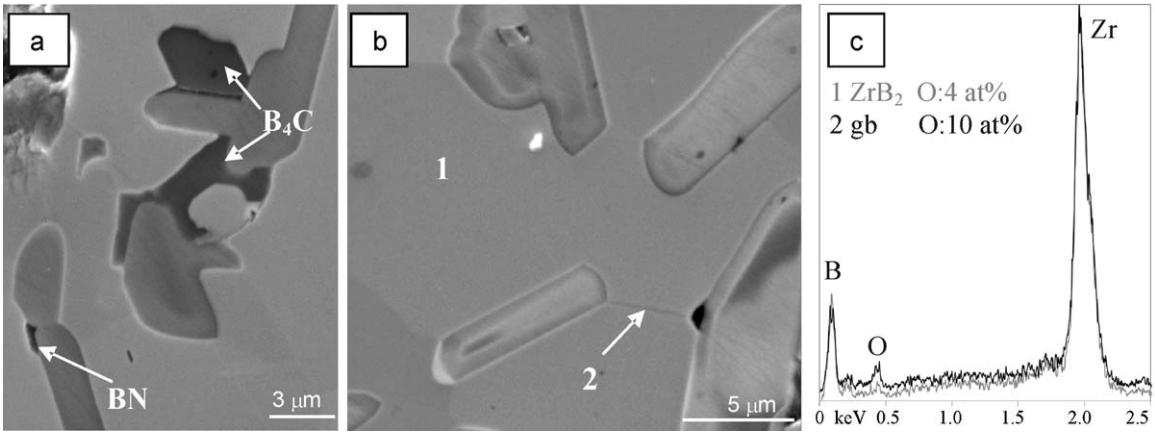


Fig. 6. SEM images of a polished section of ZSβ showing the formation of secondary phases. (a) B4C and BN, (b) Oxygen enrichment along grain boundaries. In (c) the EDS spectra of points 1 and 2 in (c) underlying the different oxygen content.

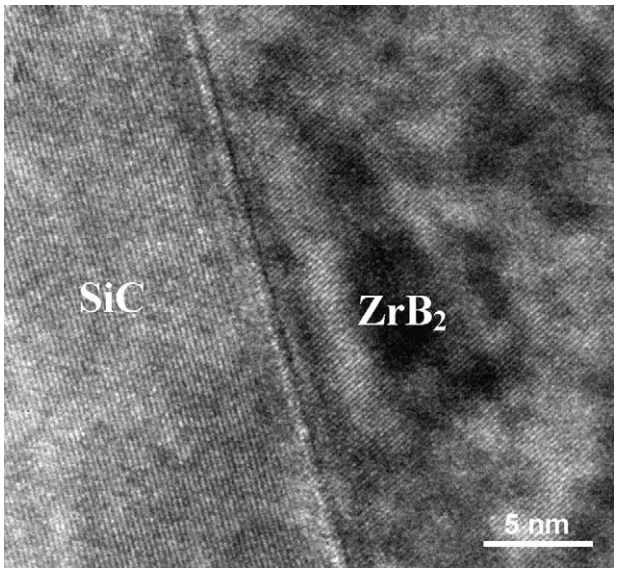


Fig. 7. TEM images showing a clean $ZrB_2$/SiC interface in ZSβ.

## 4. Discussion

### *4.1. Effect of the sintering aids on the microstructural evolution*

The results displayed so far show that with appropriate setting of composition and sintering cycle, a microstructure development of SiC platelets distributed in a $ZrB_2$ rounded matrix can be obtained starting from conventional $ZrB_2$–SiC particles powder mixtures.

Comparing the materials under investigation the most striking differences can be summarized as follows:

- Intergranular fracture for ZMα, ZMβ and transgranular fracture for ZSβ.
- Considerable $ZrB_2$ coarsening and apparently more ordered/regular distribution of SiC platelets in ZSβ (AR ∼ 3). Finer microstructure for ZMα and ZMβ, either for $ZrB_2$ grains or for SiC platelets (AR ∼ 2).
- Secondary phases like Mo–Si–B, Zr–Si, Si–O glassy phases in ZMα and ZMβ, whilst Zr–Si, BN and Si–O–N–Zr in ZSβ. $ZrB_2$–SiC interfaces apparently clean in all the materials.
- Superior mechanical properties for ZMα and ZMβ compared to ZSβ, especially in terms of fracture toughness.

Such differences are all definitely related to the change of the sintering agent, $MoSi_2$ or $Si_3N_4$. As the sintering additives affect the sintering mechanisms, the interaction between matrix and SiC particle, the final matrix microstructure and the mechanical properties, it is worth resuming the detailed effect of both sintering agents on the boride matrix.[7,20]

$MoSi_2$ was reported to help the densification in different ways. Removal of surface oxide present on boride starting particle occurs by reactions such as:

$$MoSi_2 + \text{B–Ospecies} = MoB + \text{Mo–Si–B–Ospecies} + SiO_2 \quad (1)$$

$MoSi_2$–MoB–Si–B species can locally form liquid phases at 1350 °C.[22] In the same system another eutectic temperature takes place at 1802 °C, among MoB–$Mo_5Si_3$–$MoSi_2$, and another one at 1885 °C, among Mo–MoB–$Mo_5Si_3$–$Mo_5SiB_2$.[22] Therefore, it is assumed that a small amount of liquid forms in this system, which promotes the matter transfer mechanisms. Generally, however, these phases show a poor wetting tendency towards $ZrB_2$ and, in the sintered material, crystalline $Mo_5(Si,B)_3$ phases are only found at triple points.[20] Accordingly, in the present $MoSi_2$-doped composites, $ZrB_2$/$ZrB_2$ interfaces were partially wetted and $ZrB_2$/SiC platelet interfaces were clean (Fig. 4a and b). Finally, residual silica-based phases were partially eliminated through carbo-thermal reduction in the CO-rich furnace environment. The limited amount of liquid available can also explain the less pronounced grain coarsening of $ZrB_2$ and the local agglomeration of SiC platelets, which derives from the accumulation of the original SiC particles. The possible microstructural evolution is depicted in the sketch of Fig. 8a.

As far as the $ZrB_2$–SiC–$Si_3N_4$ system is concerned, the sintering process involves the interaction of silicon nitride with

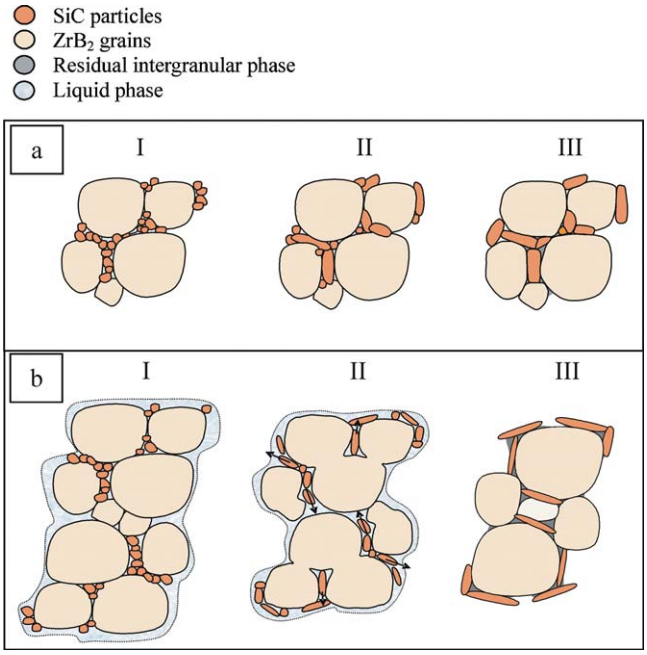


Fig. 8. Mechanism of microstructure evolution between 1900 °C and 2100 °C. For ZMβ in (a): The original SiC particles (I) undergo β → α transformation (II) and further coalescence (III) without substantial movement from the original site. For ZSβ in (b): The original SiC particles (I) are dragged by the liquid phase among the matrix (II), whilst β → α transformation of SiC particles occur. Coalescence of $ZrB_2$ grains and SiC grains results in overall coarsening (III).

residual oxides (boria and zirconia) and can be described by the following reactions[7]:

$$Si_3N_4 + 2B_2O_3 = 4BN + 3SiO_2 \quad (2)$$

$$ZrB_2 + SiO_2 + Si_3N_4 = Si\text{–}O\text{–}N\text{–}Zr_{(liquid)} \quad (3)$$

The twofold effect of the sintering aid is the removal of surface oxides from boride particles (which hinders densification) and the formation of a liquid phase which promotes matter transfer mechanisms. If the sintering process is stopped at $T < 1800$ °C, the resulting microstructure consists of $ZrB_2$ grains separated by Si–O–N–Zr glassy intergranular phases, with SiC particles agglomerates at the triple points embedded in the same Si–O–N–Zr glassy intergranular phase.[7,14] Thus, differently from ZMα and ZMβ, in ZSβ a large amount of liquid phase was available for the evolution and rearrangement of the microstructure. Prolonging the thermal treatment to 2100 °C, the $ZrB_2$ phase continued to coarsen, with larger grains growing at the expenses of smaller ones, whilst SiC particles coalesced and started to grow anisotropically. The squeezing of liquid away from coalescing boride grains caused SiC particles dragging, displacement and rearrangement, resulting in an almost regular pattern, as sketched in Fig. 8b. As for the previous systems, residual Si–O–N glassy phases were partially or totally carbothermal reduced. Simple thermodynamic calculations confirm that the elimination of Si–O–N glassy phase may occur at temperatures around 2000 °C through reaction with CO species and emission of volatile SiO, $CO_2$, NO species.

### *4.2. Effect of the sintering aids on the mechanical properties*

Considering the mechanical properties, it can be observed that the flexural strength of the composites was lower than the corresponding unreinforced matrices. This is mainly due to the presence of SiC platelets, some agglomerates of which acted as failure origins. Moreover, in case of ZSβ, the strength was further penalized by a lower density and the grain coarsening of the $ZrB_2$ matrix, see Table 1. The presence of SiC platelets and the matrix grain coarsening made the strength of all the three composites lower than the typical strength reported in the literature for similar materials, though they were almost the same of chopped fibers-reinforced materials (370–410 MPa[14,15]).

For the fracture toughness, the values obtained for ZMβ and ZMα are much higher than that of materials produced by pressureless sintering techniques and even higher than the values found for SiC particles-reinforced $ZrB_2$ produced by hot pressing, Fig. 1. The toughness of ZMβ is nearly comparable to that of whiskers- or chopped fibers-reinforced composites, Fig. 1. In this kind of composites, the toughness is determined by several microstructural factors as, for example, the residual thermal stresses and the interfacial bonding between the different phases. Whilst the toughening contribution of the residual thermal stresses in $ZrB_2$–SiC composites is slightly negative,[14,15] the matrix microstructure and the interfacial bonding can generate compensating toughening mechanisms. In order to investigate such an occurrence, the interaction between an advancing crack and the microstructure was analyzed by introducing cracks onto polished surfaces of the composites by 98.1 N Vickers indentations. The path of the cracks created in this way revealed interesting differences between the investigated materials, Fig. 9. As can be seen in Fig. 9a and b, the crack path in ZMβ was both tortuous and discontinuous. In the $ZrB_2$ matrix, the tortuosity was due to the intergranular nature of the crack. In correspondence of the SiC platelets, the tortuosity was mainly due to the impingement angle: when the crack approached the reinforcing SiC platelets at angles lower than 60°, interfacial debonding occurred and the crack circumvented the SiC platelets; for higher impingement angles, the advancing crack straightly penetrated the SiC platelets. Similar features, not shown, were also found for ZMα. In ZMα and ZMβ, the tortuosity of the crack, calculated as the ratio between the actual path length and the shortest distance between the start and end points of the crack, was about 1.5. The discontinuity of the crack was observed both in correspondence of some $ZrB_2$ grains and some SiC platelets, Fig. 9a. From these findings, therefore, crack deflection and crack pinning seem to be the most important toughening mechanisms in ZMα and ZMβ.

In ZSβ, Fig. 9c, the crack path was continuous and almost straight both in the matrix and the SiC platelets, independently of the impingement angle. The calculated tortuosity was in this case about 1. Apparently, no toughening mechanism was activated in this composite.

According to the above results, the fracture toughness of the investigated systems seems to be dictated by the interface strength among the different microstructural components

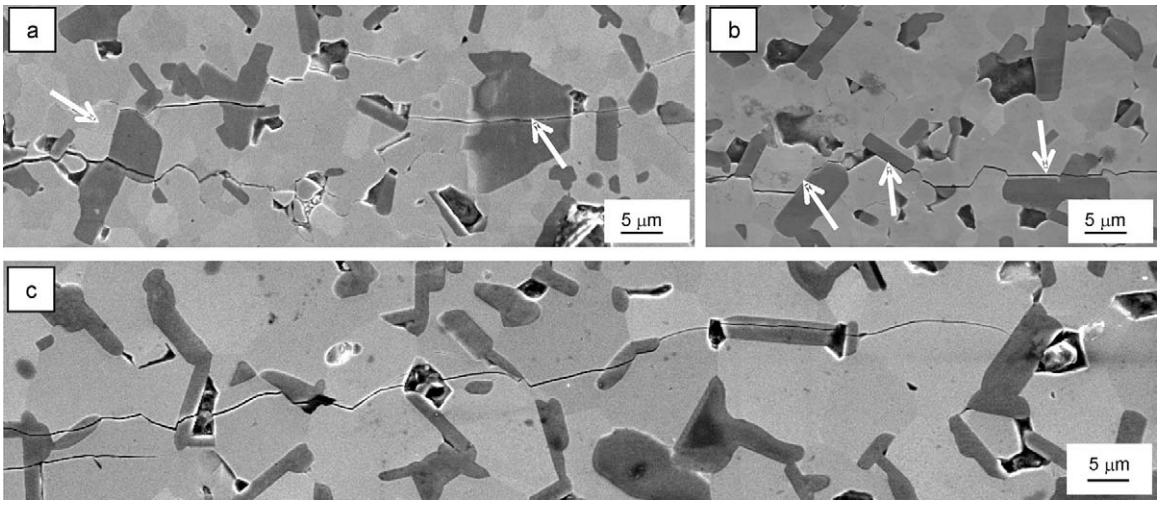


Fig. 9. Crack propagation after a 98.1 N Vickers indentation on (a) and (b) ZMβ and (c) ZSβ. The crack tip is on the right. The arrow in (a) indicates crack branching and cleavage of a SiC platelet oriented along the basal plane, in (b) the bypass of the SiC platelets oriented at low angle.

($ZrB_2$/$ZrB_2$ grains and $ZrB_2$ grain/SiC platelet). From this point of view, the straight crack path in ZSβ indicates that in this composite the interfaces were very strong and no toughening mechanism was operative. On the other hand, in the $MoSi_2$-doped composites, the interfaces were relative weaker as the crack path could deviate along the $ZrB_2$/$ZrB_2$ or $ZrB_2$/SiC interface if the impingement angle was appropriate. Several studies conducted on silicon nitride have demonstrated that interfacial debonding is primarily affected by the chemistry of the intergranular glassy phase.[23] In turn, the chemistry of the intergranular phase is affected by the choice of the sintering aid, as well as by the different impurities that contaminate the starting powders. In our two systems (the $MoSi_2$-doped one and the $Si_3N_4$-doped one), a different chemistry of the Si–O-based intergranular phase was indeed observed: one containing Mo atoms and the other one containing N atoms. However SEM and TEM analysis revealed that, in both systems, the majority of interfaces, especially those between $ZrB_2$ and SiC, were apparently clean. This suggests that the fracture properties of these systems must be influenced by the chemistry at a very small scale. Just as an indication, the presence of very thin films (less than 2 nm) or the segregation of impurities at the interfaces between the microstructural components can be mentioned. Although further work is necessary in order to assess this hypothesis, this work well evidences that even the in situ formation of elongated grains or platelets, is not always enough for achieving a significant improvement of the fracture toughness, as this property is also strongly affected by the chemistry of the grain boundaries.

### 4.3. Comparison with particle and fiber-reinforced $ZrB_2$

As a final indication, it is worthy comparing some fracture toughness values of composites as a function of reinforcement geometry. Considering composites with the same matrix material and the same reinforcement content, the fracture toughness value of the baseline matrix and those of particle-, platelet-, whisker- and chopped fiber-reinforced composites are shown in Fig. 10. A clear trend with the reinforcement geometry is

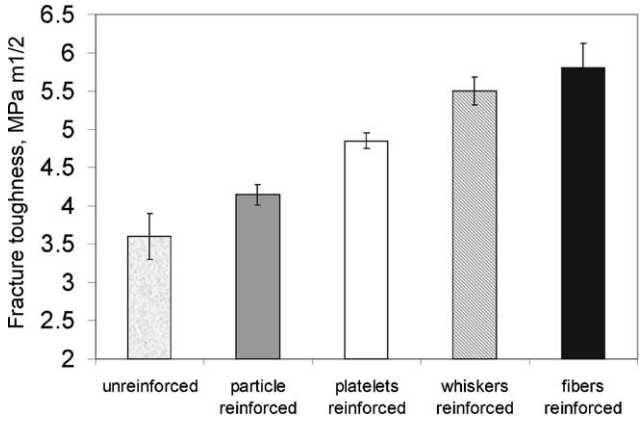


Fig. 10. Comparison of averaged fracture toughness values for different classes of composites (unreinforced and reinforced with 20 vol% particles, platelets, whiskers, chopped fibers).

self-evident: the more elongated is the reinforcement (particle → platelet → rod-shaped), the tougher is the composite, with whiskers and fibers giving nearly the same toughening contribution. At first sight, the fracture toughness trend with the reinforcement geometry shown in Fig. 10 well corresponds to the prediction of crack-deflection toughening as proposed by Faber and Evans[24] on a fracture mechanics basis. This would suggest that in these composites crack deflection is the main toughening mechanism. However, differently from particle- and platelet-composite, in the chopped-fiber composite crack deflection was not observed. The high toughness of this composite originated instead from another toughening mechanism such as crack bowing.[14,15]

## 5. Conclusive remarks

$ZrB_2$–SiC composite ceramics were pressureless sintered at 2100 °C with addition of $MoSi_2$ or $Si_3N_4$ using either α- or β-SiC in order to obtain tough $ZrB_2$–SiC platelets composites. After sintering, all the composites showed the formation of SiC

platelets, but different growth rates and microstructures which were dependent on the type of sintering aid. An almost regular pattern of SiC platelets distributed in a coarse $ZrB_2$ matrix was found for the $Si_3N_4$-doped system. A finer but more agglomerated distribution of SiC platelets was instead observed for the $MoSi_2$-doped composites. All the materials generally showed clean $ZrB_2$/SiC interfaces. These morphological features led to a substantial difference in the mechanical properties: the material containing β-SiC and $MoSi_2$ achieved a fracture toughness of 5 MPa $m^{1/2}$ and a strength of 410 MPa, which remained almost unvaried up to 1200 °C. Conversely, the material containing β-SiC and $Si_3N_4$ had a toughness of 3.8 MPa $m^{1/2}$ and strength of 300 MPa, i.e. the properties were not improved compared to the typical values of this class of materials.

This study pointed out that after a proper tuning of the starting powder, sintering aid, densification temperature and time, one can obtain in one step a material possessing a toughness comparable with $ZrB_2$-materials containing reinforcing phases such as SiC whiskers or SiC short fibers. As already observed in other toughened materials, it is fair to point out that the toughness increase was in these composites counterbalanced by a strength reduction with respect to the unreinforced matrices. The in situ toughening method has however several advantages over other conventional routes: no health hazard associated with whiskers or chopped fibers manipulation, possibility to produce near-net shaped or large-sized components, atmospheric process sintering and possibility to increase the volume of the reinforcing phase. All these benefits can contribute to considerably cut down the cost of the final material.

## Acknowledgements

The authors would like to acknowledge R. Renis and C. Melandri for samples preparation and mechanical testing. One of the author (L.S.) is very grateful to L. Ortolani for his assistance during TEM sessions.

## References

1. Fahrenholtz WG, Hilmas GE, Talmy IG, Zaykoski JA. Refractory diborides of zirconium and hafnium. *Journal of the American Ceramic Society* 2007;**90**:1347–64.
2. Chamberlain AL, Fahrenholtz WG, Hilmas GE, Ellerby DT. High strength ZrB2-based ceramics. *Journal of the American Ceramic Society* 2004;**87**:1170–2.
3. Zhu S, Fahrenholtz WG, Hilmas GE. Influence of silicon carbide particle size on the microstructure and mechanical properties of zirconium diboride–silicon carbide ceramics. *Journal of the European Ceramic Society* 2007;**27**:2077–83.
4. Sciti D, Guicciardi S, Bellosi A, Pezzotti G. Properties of a pressureless-sintered $ZrB_2$–$MoSi_2$ ceramic composite. *Journal of the American Ceramic Society* 2006;**89**:2320–2.
5. Silvestroni L, Sciti D. Effect of $MoSi_2$ additions on the properties of Hf- and Zr-$B_2$ composites produced by pressureless sintering. *Scripta Materialia* 2007;**57**:165–8.
6. Sciti D, Silvestroni L, Celotti G, Melandri C, Guicciardi S. Sintering and mechanical properties of $ZrB_2$–$TaSi_2$ and $HfB_2$–$TaSi_2$ ceramic composites. *Journal of the American Ceramic Society* 2008;**91**:3285–91.
7. Monteverde F, Guicciardi S, Bellosi A. Advances in microstructure and mechanical properties of zirconium diboride based ceramics. *Materials Science and Engineering A* 2003;**346**:310–9.
8. Munz D, Fett T. *Ceramics: mechanical properties, failure behavior, materials selection*. Berlin: Springer-Verlag; 1999.
9. Watts J, Hilmas GE, Farenholtz WG, Brown D, Clausen B. Stress measeurements in $ZrB_2$–SiC composites using Raman spectroscopy and neutron diffraction. *Journal of the European Ceramic Society* 2010;**30**:2165–71.
10. Zhang P, Hu P, Zhang X, Han J, Meng S. Processing and characterization of $ZrB_2$–SiCw ultra-high temperature ceramics. *Journal of Alloy and Compounds* 2008;**472**:358–62.
11. Wang H, Wang CA, Yao X, Fang D. Processing and mechanical properties of zirconium diboride-based ceramics prepared by spark plasma sintering. *Journal of the American Ceramic Society* 2007;**90**:1992–7.
12. Zhang X, Xu L, Du S, Han W, Liu C, Han J, et al. Microstructure and properties of silicon carbide whisker reinforced zirconium diboride ultra-high temperature ceramics. *Solid State Science* 2008;**11**:156–61.
13. Yang F, Zhang X, Han J, Du S. Characterization of hot-pressed short carbon fiber reinforced $ZrB_2$–SiC ultra-high temperature ceramic composites. *Journal of Alloy and Compounds* 2009;**472**:395–9.
14. Silvestroni L, Sciti D, Guicciardi S, Melandri C. Toughened $ZrB_2$-based ceramics with addition of SiC whiskers or chopped fibres. *Journal of the European Ceramic Society* 2010;**30**:2155–64.
15. Guicciardi S, Silvestroni L, Nygren M, Sciti D. Microstructure and toughening mechanisms in spark plasma sintered $ZrB_2$ ceramics reinforced by SiC whiskers or SiC chopped fibers. *Journal of the American Ceramic Society* 2010;**93**(8):2384–91.
16. Zou J, Zhang G-J, Kan Y-M. Formation of tough interlocking microstructure in $ZrB_2$–SiC based ultrahigh-temperature ceramics by pressureless sintering. *Journal of Materials Research* 2009;**24**(7):2428–34.
17. Padture NP. In situ-toughened silicon carbide. *Journal of the American Ceramic Society* 1994;**77**:519–23.
18. Munz DG, Shannon Jr JL, Bubsey RT. Fracture toughness calculations from maximum load in four point bend tests of chevron notch specimens. *International Journal of Fracture* 1980;**16**:R137–41.
19. Telle R. Boride and carbide ceramics. In: Cahn RW, Haasen P, Kramer EJ, editors. *Materials science and technology*. Weinheim: Verlag Chemie; 1993. p. 206.
20. Silvestroni L, Kleebe H-J, Lauterbach S, Müller M, Sciti D. Transmission electron microscopy on Zr- and Hf-borides with $MoSi_2$ addition: densification mechanisms. *Journal of Materials Research* 2010;**25**(5):828–34.
21. Medri V, Capiani C, Bellosi A. Properties of slip-cast and pressureless sintered $ZrB_2$–SiC composites. *International Journal of Applied Ceramic Technology* 2011;**8**(2):351–9.
22. Katrych S, Grytsiv A, Bondar A, Rogl P, Velikanova T, Bohn M. Structural materials: metal–silicon–boron. On the melting behaviour of Mo–Si–B alloys. *Journal of Alloy and Compounds* 2002;**347**:94–100.
23. Sun EY, Becher PF, Pluckett KP, Hsueh CH, Alexander KB, Waters SB, et al. Microstructural design of silicon nitride with improved fracture toughness. II. Effects of yttria and alumina additives. *Journal of the American Ceramic Society* 1998;**81**:2831–40.
24. Faber KT, Evans AG. Crack deflection processes. 1. Theory. *Acta Metallurgica* 1983;**31**:565–76.